(Submitted to JGR Planets, 01 September 1997; Revised 16 March 1998)

AMMONIA ABUNDANCE IN JUPITER'S ATMOSPHERE DERIVED FROM THE ATTENUATION OF THE GALILEO PROBE'S RADIO SIGNAL

W. M. Folkner, R. Woo and S. Nandi

Jet Propulsion Laboratory
California Institute of Technology
Pasadena, California 91109

Abstract

The radio signal from the Galileo probe to the orbiter experienced attenuation due to ammonia in Jupiter's atmosphere during the probe descent. A profile of the ammonia content as a function of depth in the atmosphere has been derived from the measurements of the attenuation. The derived ammonia abundance rises to a molar fraction of 700 ± 100 parts-per million for pressures greater than 7 bar, about four times that expected based on the solar abundance of nitrogen.

Introduction

On 7 December 1995 the Galileo probe entered the atmosphere of Jupiter. The Galileo probe used two radio channels transmitting at 1387 MHz to send its engineering and science data to the Galileo orbiter. The amplitude of the signal received at the orbiter was sampled at a high rate (47 ms) in order to study scintillation, turbulence, and refractive-index fluctuations in Jupiter's atmosphere. Similar measurements were made with the Pioneer Venus probes (Woo et al. 1979). The complicated motion of the probe suspended under its parachute during the descent introduced systematic variability at the same time scale as the expected scintillation, making it impossible to separate the scintillations from changes in amplitude caused by changes in the probe orientation.

Slowly varying amplitude changes could be reliably measured. Thus measurements of the amplitude of the probe radio signal allowed the investigation of some constituents of Jupiter's atmosphere that attenuated the signal. Clouds would be expected to attenuate the signal if the probe had descended through them. However the probe entered a relatively cloud-free region of Jupiter. Instruments on the probe able to measure cloud properties detected no significant clouds in the region below a level corresponding to a pressure of about 1.5 bar (Ragent et al., 1996; Sromovsky et al. 1996; 1998). Besides clouds, the only atmospheric constituent expected to cause significant attenuation of the probe signal is ammonia. The attenuation due to other constituents, such as water and hydrogen sulfide, was negligible at the concentrations measured by the probe's mass spectrometer (Niemann et al. 1996; 1998). The observed attenuation and the inferred profile of ammonia content in Jupiter's atmosphere are given below.

Experiment description

The received radio signal power depended on a number of instrumental and geometric parameters. The geometry of the radio link is shown in Figure 1. The probe moved faster in longitude than the orbiter during the descent, with the orbiter and the probe at the same longitude about 17 minutes into the descent. There was about 2.2° difference in the probe and orbiter latitudes. The power received by the orbiter, P_R, is given by

$$P_R = G_A G_R G_S G_T P_T \qquad (1)$$

where P_T is the power transmitted, G_T is transmitting antenna gain, G_S is the 'space loss' due to the distance between the probe and orbiter, G_R is the receiving antenna gain, and G_A is the loss due to atmospheric absorption. Each term is described below. Probe transmission began about 190 seconds past entry, where time of entry is defined as the time that the probe was 450 km above the 1-bar pressure level. The orbiter receiver locked on the probe signal about 34 s later. The probe data and orbiter power measurements are referred to a reference time according to the probe clock which was 166 s after entry. The pressure, temperature and altitude as a function of time were determined by the probe Atmospheric Structure Instrument and are given by Seiff et al. (1996; 1998).

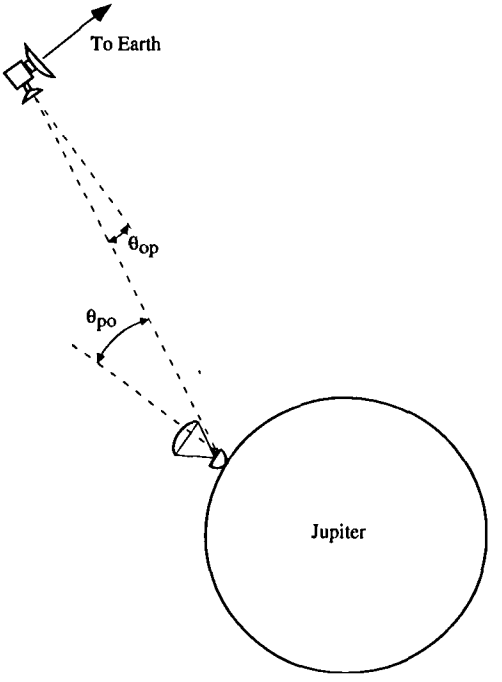

Figure 1. Geometry of the probe-orbiter radio link.

One of the probe's two radio channels was left-circularly polarized (LCP) at 1387.0 MHz and the other right-circularly polarized (RCP) at 1387.1 MHz. The power transmitted by each channel was monitored on the probe and the power measurements were transmitted to the orbiter as part of the

telemetry stream. Figure 2 shows the measured transmitted power for each channel over the probe descent and values are given in Table 1. As the probe descended, the temperature of the electronics changed more than had been expected before flight. Both transmitters experienced difficulties about 45 minutes past entry, when the surrounding pressure was about 14 bar and the ambient temperature was 370 K. The LCP transmitter experienced a sharp drop in power followed by a gradual degradation, while the RCP channel failed abruptly.

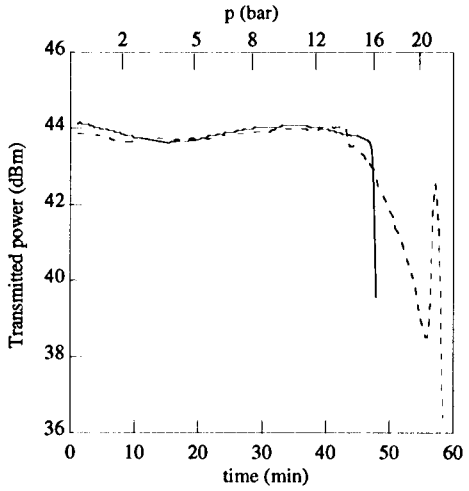

Figure 2. Transmitted power from the probe RCP (solid line) and LCP (dashed line) channels during probe descent.

Both channels were fed to an antenna fixed to the top of the probe, pointing through the parachute and roughly towards the orbiter. The probe antenna was a crossed-dipole with a half-power beam width θ_{pw} of 56°. As the apparent position of the orbiter changed during the descent, the probe pointing angle θ_{po} between the average antenna axis (local vertical) and the direction to the orbiter varied. The time history of the probe pointing angle is shown in Figure 3 and listed in Table 1. The nominal gain of the probe antenna in the direction of the orbiter is computed by

$$G_T(\text{dB})=9.6+20\ \log[\sin(2.783\ \theta_{po}/\theta_{pw})/(2.783\ \theta_{po}/\theta_{pw})] \quad (2)$$

The resulting probe antenna gain is shown in Figure 3.

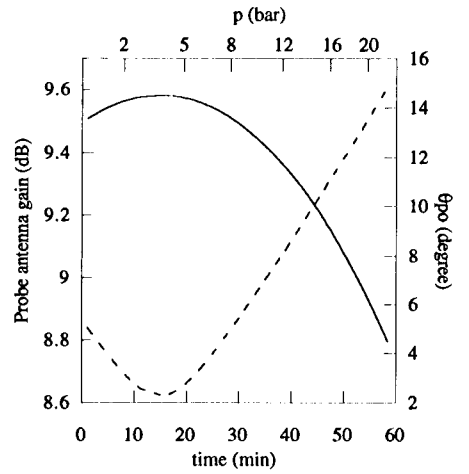

Figure 3. Probe antenna gain (solid line) and pointing angle (dashed line) during probe descent.

The distance between the probe and orbiter increased throughout the probe descent. The 'space loss' of the signal is given by

$$G_S = \lambda^2 / (4\pi r)^2 \quad (3)$$

where λ is the radio wavelength and r is the distance between the probe and the orbiter. The time history of the distance r, based on the reconstructed probe and orbiter trajectories, is shown in Figure 4. The computed space loss is given in Table 1 and also shown in Figure 4.

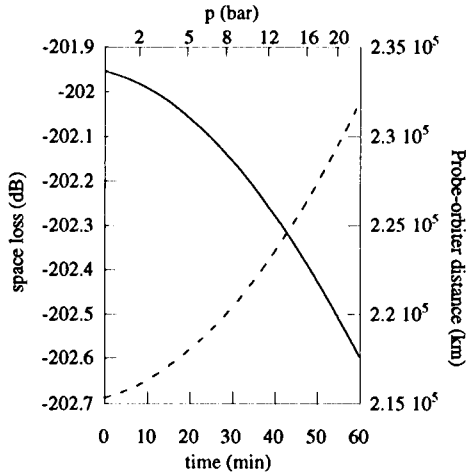

Figure 4. Probe-orbiter distance (dashed line) and the resulting space loss (solid line) during the probe descent.

The orbiter received both probe radio channels through a 1.1 m diameter parabolic antenna, with a half-power beam width θ_{ow} of 12.6°. The orbiter antenna was held fixed for the first 22 minutes of the probe descent, and adjusted at several discrete times later during the probe descent. The pointing actuator resolution was 0.5°. The uncertainty in the pointing was estimated to be 0.7° (1σ) (Neff 1994). The orbiter pointing angle θ_{op} between the orbiter antenna axis and the direction to the probe is tabulated in Table 1 and shown in Figure 5. The nominal gain of the orbiter antenna in the direction of the probe is computed by

$$G_R(\text{dB})=20.8+20\ \log[\sin(2.783\ \theta_{op}/\theta_{ow})/(2.783\ \theta_{op}/\theta_{ow})] \quad (4)$$

The nominal orbiter antenna gain is shown in Figure 5.

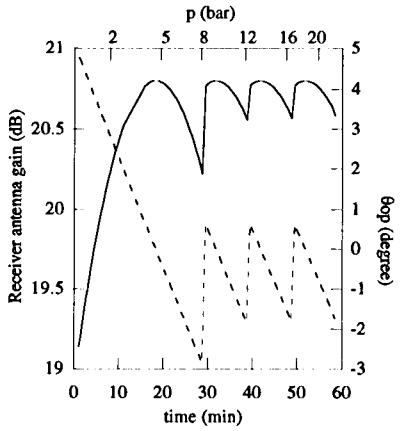

Figure 5. Orbiter antenna gain (solid line) and pointing angle (dashed line) during probe descent.

The probe transmission was 100% phase modulated with up to 512 phase transitions per second to encode telemetry at 256 bits/s. The orbiter receiver sampled the signal amplitude 8 times per bit and averaged over 12 bits to form one power measurement. The received power measurements were stored on the orbiter's tape recorder and later relayed to Earth. Not all of the received power measurements were successfully relayed, leaving one gap of several minutes and a few shorter gaps.

The bit rate was based on the probe's reference oscillator. Variation in the probe-orbiter relative velocity caused a varying Doppler shift, which resulted in the time boundaries of the probe telemetry bits drifting with respect to the orbiter reference clock. This caused a quasi-periodic signature in the received power measurements as the number of bits sampled by the orbiter receiver at its clock rate corresponding to a varying fractional number of transmitted bits. This 'scalloping' had been observed during check out of the probe and orbiter radio systems and was well understood. The scalloping effect can bee seen in the short section of received power measurements shown in Figure 6. The size of the effect was of order 0.5 dB over time scales of about 100 s. The time scale is indicative of the rate difference between the orbiter clock and the received bit streem. The maximum in the signature occurred when the probe bit stream was best aligned with the orbiter clock. The scalloping was removed by fitting a function of the form

$$A\cos[\pi(t-T_a)/T_w] \qquad (5)$$

to the data, solving for the amplitude of the scallop A, the time of the peak of the scallop T_a, and the period of the scallop T_w (Linkchorst 1996). Because each scallop was well sampled, and the functional form understood, the scallop fit was limited only by the effective data noise. The scalloping removal does not significantly affect the interpretation of atmospheric attenuation.

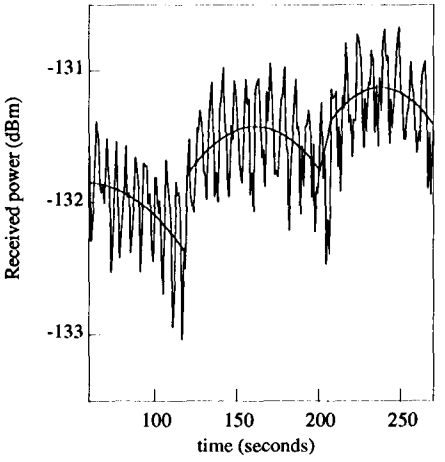

Figure 6. Observed time dependence of the amplitude of the Galileo probe radio signal as received by the orbiter. Each point represents an average of 20 samples taken at 47 ms intervals. Also shown is a fit to the systematic scalloping caused by differences in probe and orbiter clock rates.

Several shorter period signatures were also observed in the power measurements, as can been seen in a sample of the data shown in Figure 6. There were (typically) two quasi-periodic signatures. One is thought to be to due to the rotation of the probe about the axis connecting the probe to the parachute. The variation in power induced by this rotation was caused by azimuthal asymmetry of the probe antenna pattern. The other signature seen in the amplitude data is thought to be related to the pendulum motion of the probe swinging on its tether below the parachute. Figure 7 shows a series of power spectra formed from two-minute portions of the amplitude data. The amplitude of the variation due to rotation diminished as the angle between the antenna axis and the direction to the probe decreased, since the probe antenna pattern was more symmetric nearer the antenna axis. The period of the signature identified with the probe rotation was initially ~6 s, slowing to ~14 s 20 minutes after entry and ~50 s at the end of the probe lifetime. The period associated with the probe swinging was about 4 s, with some variation as a function of pressure. A signature period half that of the 'swinging' period is also sometime evident. The swinging period was slightly faster than the 4.9 s calculated based on simple pendulum motion of the probe suspended by a tether of length ~13.9 m (Seiff et al. 1996).

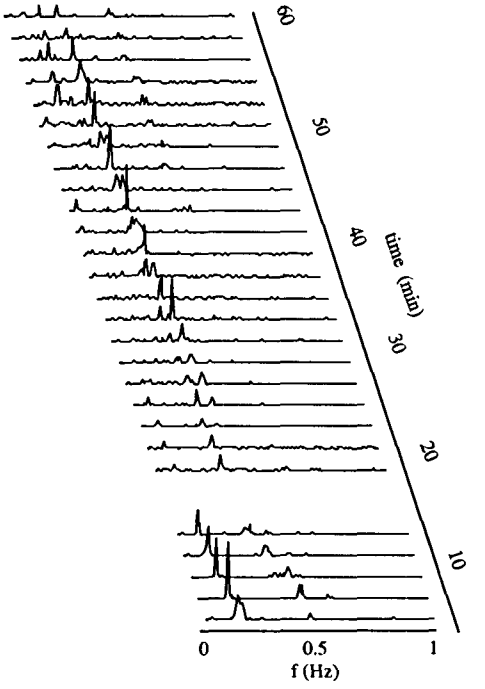

Figure 7. Series of power spectra of the amplitude of the Galileo probe radio signal as received by the orbiter. Each spectrum was formed from 2 minutes of amplitude data.

Figure 8 shows the full history of the received power measurements, using averages over 20 s of samples to remove the quasi-periodic signatures. A constant offset is evident between the RCP and LCP received power. This could be due to a number of instrumental effects, such as an uncalibrated cable insertion loss between the receiver antenna and the amplifier. An unknown constant loss precludes assessment of atmospheric absorption above the altitude of the probe at the time of the first received power measurements. The unknown constant loss does not affect the derived atmospheric absorption for lower altitudes, which is based on changes in the received power.

The loss of probe signal power due to atmospheric loss, derived by subtracting the known effects from the received power, is

shown in Figure 9. The attenutation has been converted to that expected through a vertical path by dividing by $cos\theta_{po}$. A constant offset has been removed from each channel. Also shown in Figure 9 is the signal attenuation expected from absorption by ammonia, as calculated below, based on an ammonia abundance (relative to hydrogen) consistent with that found in the sun. The observed attenuation is clearly larger than this, especially for pressures greater than 6 bar. The derived atmospheric losses for the two channels agree well for about the first 42 minutes, down to the 14 bar level. At that time the LCP transmitted power readings dropped abruptly and then declined slowly through about 58 minutes, when the probe was at a pressure of 22.5 bar. The RCP transmitter power showed no changes at 42 minutes, but failed at about 48 minutes, when the pressure was 16 bar.

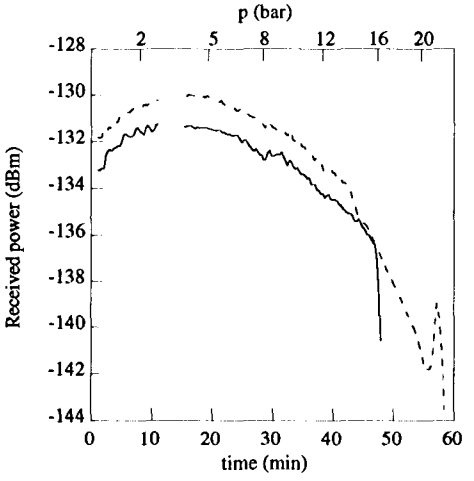

Figure 8. Power received by the orbiter for the RCP(solid line) and LCP (dashed line) channels. Each point represents an average of 400 samples at 46 ms intervals.

For the first few minutes, down to a pressure of about 2 bar, Figure 9 shows a slight increase in signal. This is most likely due to an error in the orbiter antenna pointing. At the beginning of the probe descent the probe was the farthest from the orbiter antenna axis, where the sensitivity to pointing errors was largest. After the probe reached the 2-bar level, the probe was kept within 3° of the orbiter antenna axis and the error due to pointing was smaller. Corrections to the orbiter antenna pointing can be estimated from the measurements of received amplitude, largely because of discontinuities introduced at the probe re-pointing times. The pointing corrections and residual errors are included as part of the ammonia profile retrieval.

Atmospheric attenuation

The absorption of radio signals by ammonia is due to molecular transition resonances. The absorption coefficient α at frequency ν is given by

$$\alpha = n\sum_j S_j(T)F(\nu,\nu_j) \qquad (6)$$

where the summation is over transitions, n is the number density of ammonia molecules, $S_j(T)$ is the line intensity at temperature T, and $F(\nu,\nu_j)$ describes the shape of the resonance line with resonant frequency ν_j. The line intensities and frequencies are given by Poynter and Kakar (1975). In Jupiter's atmosphere the ammonia resonances are Doppler-broadened by collisions, mainly with hydrogen and helium molecules. The absorption by ammonia mixed with amounts of hydrogen and helium approximating Jupiter's atmosphere has been measured in a number of laboratory experiments (Morris and Parsons 1970; Steffes and Jenkins 1987; Spilker 1990; Joiner and Steffes 1991). The line-shape factor derived by Ben-Reuven (1965; 1966) has been used successfully to fit these measurements (Berge and Gulkis 1976; Spilker 1990; Joiner and Steffes 1991). The line-shape parameter is given by

$$F(\nu,\nu_j) = \frac{2}{\pi}\frac{\nu}{\nu_j}\frac{(\gamma_j-\varsigma_j)\nu^2+(\gamma_j+\varsigma)(\nu_j^2+\gamma_j^2-\varsigma_j^2)}{(\nu^2-\nu_j^2-\gamma_j^2+\varsigma_j^2)^2+4\nu^2\gamma_j^2} \qquad (7)$$

where the coefficients γ_j and ς_j are given by

$$\begin{aligned}\gamma_j &= AP_{H_2}\tau^{2/3} + BP_{He}\tau^{2/3} + CP_{NH_3}w_j\tau \\ \varsigma_j &= DP_{H_2}\tau^{2/3} + EP_{He}\tau^{2/3} + FP_{NH_3}w_j\tau\end{aligned} \qquad (8)$$

where $\tau = (300/T)$, P_{H_2}, P_{He}, and P_{NH_3} are the partial pressures of hydrogen, helium, and ammonia, w_j is the self-broadened resonant line width (Poynter and Kakar 1975), and *A, B, C, D, E,* and *F* are coefficients, possibly as a function of pressure and temperature, fit to the laboratory measurements. At the frequency of the probe radio signal, and the pressures and temperatures measured during the probe descent, the line-shape fits by Joiner and Steffes (1991) and by Spilker (1990) agree to better than 5%.

It is convenient to reference the ammonia abundance to a 'solar' value, which is characterized by the ratio of nitrogen to hydrogen atoms in the sun. Here we adopt the ratio N/H to be 1.0×10^{-4} (Grevesse et al. 1990). This, combined with the determination of the mole fraction of helium of 0.135 by the probe mass spectrometer and helium abundance detector (Niemann et al. 1996; von Zahn and Hunten, 1996), gives an ammonia mole fraction of 1.7×10^{-4}. The absorptivity at the probe radio frequency expected from this amount of ammonia, based on the line-shape fit of Spilker (1990), is shown in Figure 10.

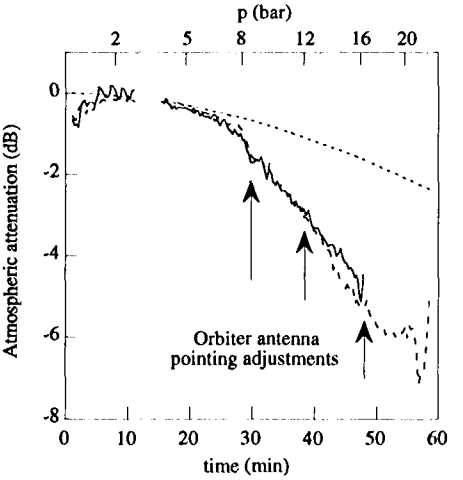

Figure 9. Atmospheric attenuation of the probe radio signal for the RCP (solid line) and LCP (dashed line) channels. The attenuation expected from ammonia at solar abundance is also shown (dotted line).

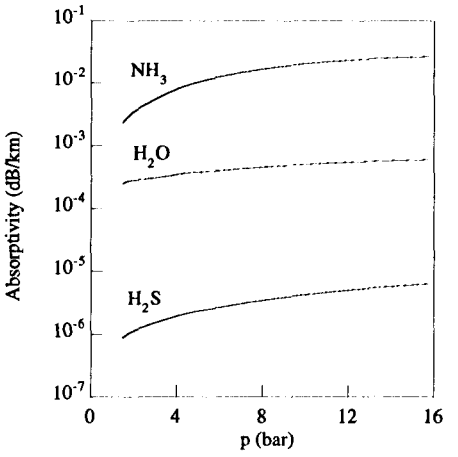

Figure 10. Absorptivity of ammonia, hydrogen sulfide, and water in Jupiter's atmosphere based on solar abundances with respect to hydrogen

Attenuation of the probe radio signal could be caused by constituents besides ammonia. Clouds are one possible source of absorption. Since no significant clouds were found at pressures between 1.5 bar and 20 bar, we assume that the absorption by clouds was negligible. Besides ammonia, the atmospheric components with the most significant absorption are thought to be hydrogen sulfide and water. The absorption by water can be calculated according to the expression by Goodman (1969). The absorptivity expected from water based on a solar ratio of oxygen to hydrogen atoms of 8.5×10^{-4} (Anders and Grevesse, 1989) is shown in Figure 10. The actual amount of water as determined by the probe's mass spectrometer was less than solar, so the attenuation by water is negligible compared with that due to ammonia. The absorption due to hydrogen sulfide can be calculated in a manner similar to that for ammonia, using fits to data by DeBoer and Steffes (1994) and hydrogen sulfide line parameters given by Poynter and Picket (1985). The absorptivity expected from hydrogen sulfide based on a solar ratio of sulfur to hydrogen atoms of 1.6×10^{-5} (Anders and Grevesse, 1989) is shown in Figure 10. Even though the actual amount of hydrogen sulfide as determined by the probe's mass spectrometer was up to three times this solar value, the attenuation is negligible compared with that due to ammonia.

Ammonia Retrieval

Since no other atmospheric component has been identified as a significant source of attenuation of the probe radio signal, we assume that the observed attenuation is entirely due to ammonia. To solve for the ammonia abundance, the attenuation data were divided into subsets corresponding to discrete layers in altitude. The attenuation for each data point was calculated using a constant ammonia mole fraction in each layer, using the formalism described above and using the ammonia line-shape factor fit by Spilker (1990). The path length through the Jovian atmopshere was derived from the determination of altitude versus time provided by the atmospheric structure instrument (Seiff et al. 1998), corrected for the path difference between vertical and the line of sight from the probe to the orbiter ($cos\theta_{po}$). The ammonia concentration by layer was estimated using an iterative weighted least-square fit. The data weights were determined from the post-fit data scatter. The number of layers was selected such that the statistical error for each layer was comparable to systematic effects discussed below. A constraint requiring the abundance parameters to be non-negative was applied. In addition to solving for ammonia abundance in the layers, a systematic correction to the orbiter antenna pointing was estimated. This is possible because at the times of the re-pointing of the orbiter antenna, discontinuities can be seen in the received power measurements. A pointing correction of 0.5° removes the observed discontinuities.

Data from both channels was included in the fit through the time that the transmitted power in the LCP showed a sharp drop. After this point the derived attenuation from the two channels disagree. Past that time, the observed attenuation from the RCP channel is consistent with the immediately preceding times, while that from the LCP channel was not. We assume that the measured transmitted power of the LCP channel experienced some sort of failure when the sharp drop occurred, and include no data from that channel after that time. Our fit included data from the RCP channel though the loss of that transmitter.

The resulting ammonia abundance profile is given Figure 11. The uncertainties indicated account for the statistical uncertainty due to the observed post-fit data scatter and for estimated systematic errors. The post-fit data scatter, for measurements averaged over 20 s, is 0.13 dB for the first layer and 0.09 dB for the other layers. The scatter is caused by a number of effects, including noise in the measurements of transmitted and received power and in fluctuations in the probe antenna pointing due to swinging and rotation of the probe.

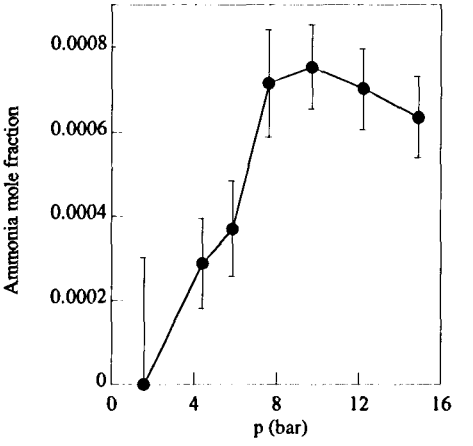

Figure 11. Estimated molar fraction of ammonia versus pressure.

The uncertainty in the pointing of the orbiter antenna is a major systematic error. A constant correction has been estimated from the data. With the assumed data noise, the statistical uncertainty in the estimated correction angle is 0.05°. At this level errors associated with the orbiter antenna pointing would be small compared with the assumed level of statistical noise. However there could be separate pointing errors associated with each re-pointing of the orbiter antenna, especially since the pointing actuators had resolution of only 0.5°. There is not sufficient signature in the data to estimate pointing corrections for each pointing interval. So the estimate of the uncertainty in the retrieved ammonia abundance accounts for a 0.5° uncertainty in the orbiter antenna pointing. This amounts to about 10% uncertainty in the retrieved ammonia abundance, except for the first layer which is more sensitive to orbiter antenna pointing

errors since the data taken during that time were relatively far from the antenna axis.

The attenuation due to ammonia has been calculated based on fits of molecular line-shapes to values measured in the laboratory. Because the attenuation at the probe signal frequency is relatively low, the line-shape fits rely more on measured absorption at higher frequencies. The extrapolation to the probe frequency should be good since it is well below the molecular resonant frequencies. Based on comparison of the published line-shape fits of Spilker (1990) and Joiner and Steffes (1991) to more recent, unpublished absorption measurements near the probe frequency, the uncertainty in the absorption calculation is estimated to be 10% (T. Spilker, private communication, 1998).

Other systematic effects could be caused by biases in the probe antenna pointing, transmitted power measurements, distance between the probe and orbiter, and received power measurements. The independent measurements of transmitted and received power in the two probe radio channels are in good agreement for the data included in our fit, which provides some confidence that systematic errors are small compared with other effects. A systematic probe antenna pointing uncertainty could be due to errors in the probe position and to tilt caused by wind shear. The probe latitude and longitude uncertainties as established by the Galileo navigation team are less than 0.1°. The wind speed derived from Doppler measurements of the probe radio signal was fairly constant below the 2-bar level (Atkinson et al. 1996; 1997). The probe tilt due to the observed wind variations is less than 0.2°. Uncertainties in the derived ammonia abundance due to probe antenna pointing errors of less than 0.5° are negligible compared with the orbiter antenna point errors, since the probe antenna patterns was wider and the nominal pointing angle was smaller. Uncertainties in the probe altitude and probe-orbiter distance are a few km or less, and their effect on the derived ammonia abundance is also negligible.

Interpretation

The derived ammonia abundance increases from a small (and uncertain) initial value to a mole fraction about 4 times solar (with respect to hydrogen) for pressures greater than 6 bar. This increase with depth is similar to the increase with depth in the abundance of water and hydrogen sulfide derived by the probe's mass spectrometer (Niemann et al. 1998). (The mass spectrometer determined an upper bound of the ammonia abundance of 7-10 times solar.) The hydrogen sulfide abundance as determined by the mass spectrometer was found to increase from a small value to about 3 times solar for pressures greater than 15 bar, while water abundance increased to about 0.3 times solar at 19 bar. This increase in abundance with depth of these volatiles may be caused by a downdraft at the probe entry site, which would suppress the volatile abundances in the upper part of the atmosphere (Atreya et al. 1997; Showman and Ingersoll 1998).

The derived ammonia abundance at depth is surprisingly high. Simple models of the formation of Jupiter predict a depletion of nitrogen with respect to the solar value (Mizuno 1980; Pollack and Bodenheimer, 1989). Other determinations of the Jovian ammonia abundance come from Voyager occultation measurements and from Earth-based microwave spectroscopy. The Voyager occultation experiments derived an ammonia abundance for pressures from 0.3 bar to 1 bar, with an abundance at 1 bar of about 1.3 times solar (Lindal et al. 1981). Microwave spectra of Jupiter are consistent with an ammonia abundance of 1-1.5 times solar for pressures greater than 1 bar (De Pater and Massie 1985). Since the microwave spectra, and possibly the Voyager occultation, presumably measured a well-mixed average of the Jovian atmosphere, their values might be expected to represent a global average ammonia abundance lower than that determined by the attenuation of the probe radio signal. However, the probe net flux radiometer experiment, while not able to determine ammonia abundance explicitly, is consistent with an ammonia abundance significantly greater than solar, and a water abundance less than solar, at high pressures (Sromovsky et al. 1998).

We conclude that the ammonia abundance at the Galileo probe site, for pressures greater than 7 bar, is 4 ± 0.5 times the solar nitrogen abundance. The apparent discrepancy with ground based measurements is not yet understood. Future measurements and theoretical analysis are needed to better determine the average abundance of nitrogen in the Jovian atmosphere.

Acknowledgment

We would like to thank the Galileo probe project personnel, especially Terry Grant, and Hughes Research Lab personnel, especially Fred Linkchorst, Dan Carlock, and Pete Garriga, for their assistance in processing the probe amplitude data. We also thank Al Seiff for providing reference pressures and temperatures prior to publication, T. Spilker for assistance with calculations of atmospheric absorption and access to unpublished laboratory measurements, and Glenn Orton and the Galileo probe science team for helpful discussions. The research described in this paper was, in part, carried out by the Jet Propulsion Laboratory, California Institute of Technology, under a contract with the National Aeronautics and Space Administration.

References

Anders, E. and N. Grevesse, Abundances of the elements; meteoritic and solar, Geochim. Cosmoshim. Acta 53, 197-214, 1989.

Atkinson, D. H., J. B. Pollack, and A. Seiff, Galileo Doppler measurements of the deep zonal winds at Jupiter, Science 272, 842-843, 1996.

Atkinson, D. H., A. P. Ingersoll, and A. Seiff, Deep winds on Jupiter as measured by the Galileo probe, Nature 388, 649-650, 1997.

Atreya, S., M. H. Wong, T. Owen, H. Niemann, and P. Mahaffy, Chemistry and clouds of the atmosphere of Jupiter: a Galileo perspective, in *The Three Galileos: The Man, the Spacecraft, the Telescope*, (C. Barbieri, J. Rahe, T. Johnson, A. Sohus, eds.), pp. 249-260, Kluwer Academic, Dordrecht, 1997.

Ben-Reuven, A., Transition from resonant to nonresonant line shape in microwave absorption, Phys. Rev. Lett, 14, 349-351, 1965.

Ben-Reuven, A., Impact broadening of microwave spectra, Phys. Rev. 145, 7-22, 1966.

Berge, G. L. and S. Gulkis, Earth-based radio observation of Jupiter; millimeter to meter wavelengths, in *Jupiter*, T.

Gehrels ed., pp. 621-692, Univ. of Arizona Press, Tucson, Arizona, 1976.

DeBoer, D. R. and P. G. Steffes, Laboratory measurements of the microwave properties of H2S under simulated Jovian conditions with applications to Neptune, Icarus 109, 352-366, 1994.

DePater, I. and S. T. Massie, Models of the millimeter-centimeter spectra of the giant planets, Icarus, 62, 143-171, 1985.

Goodman, G. C., Models of Jupiter's atmosphere, Ph. D. dissertation, University of Illinois, Urbana, Illinois, 1969.

Grevesse, N., D. L. Lambert, A. J. Sauval, E. F. van Dishoeck, C. B. Farmer, and R. H. Norton, Identification of solar vibration-rotation lines of NH and the solar nitrogen abundance, Astron. Astrophys. 232, 225-230, 1990.

Joiner J., and P. G. Steffes, Modeling of Jupiter's millimeter wave emission utilizing laboratory measurements of ammonia opacity, JGR, 96, 17463-17470, 1991.

Lindal, G. F. G. E. Wood, G. S. Levy, J. D. Anderson, D. N. Sweetnam, H. B. Hotz, B. J. Buckles, D. P. Holmes, P. E. Dome, V. R. Eshleman, G. L. Tyler, and T. A. Croft, The atmosphere of Jupiter: an analysis of the Voyager radio occultation measurements, JGR, 86, A10, 1981.

Linkchorst, F. in Galileo Probe Mission Operations Final Report, Hughes Spacecraft Co. Report HSC 960892, 1996.

Mizuno, H., Formation of the giant planets, Prog. Theo. Phys. 64, 544, 1980.

Morris, E. C. and R. W. Parsons, Microwave absorption by gas mixtures at pressures up to several hundred bars, Aust. J. Phys. 23, 335-349, 1970.

Neff, J. (ed.). Galileo Probe-Orbiter Relay Link Integration Report, JPL Pub. D-1038 Rev. C, Jet Propulsion Laboratory, California Institute of Technology, 1994.

Niemann, H. B., S. K. Atreya, G. R. Carnigan, T. M. Donohue, J. A. Haberman, D. N. Harpold, R. E. Hartle, D. M. Hunten, W. T. Kasprzak, P. R. Mahaffy, T. C. Owen, N. W. Spencer, and S. H. Way, The Galileo probe mass spectrometer: composition of Jupiter's atmosphere, Science, 272, 846-849, 1996.

Niemann, H. B., S. K. Atreya, G. R. Carnigan, T. M. Donohue, J. A. Haberman, D. N. Harpold, R. E. Hartle, D. M. Hunten, W. T. Kasprzak, P. R. Mahaffy, T. C. Owen, N. W. Spencer, and S. H. Way,, The composition of the Jovian atmosphere as determined by the Galileo probe mass spectrometer, JGR (this issue) 1998.

Pollack, J. B., and P. Bodenheimer, in *Origins and evolution of planetary and satellite atmospheres*, S. Atreya ed., Univ. Arizona Press, Tucson, Arizona, 1989,

Poynter, R. L., and R. K. Kakar, The microwave frequencies, line parameters, and spectral constants for 14NH3, Astrophys. Sup., 29, 87-96, 1975.

Poynter, R. L., and H. M. Pickett, Submillimeter, millimeter, and microwave spectral line catalog, Appl. Optics 24, 2235-2240, 1985.

Ragent, B., D. S. Colburn, P. Avrin, and K. A. Rages, Results of the Galileo probe nephelometer experiment, Science, 272, 854-856, 1996.

Seiff A. D., D. B. Kirk, T. C. D. Knight, J. D. Mihalov, R. C. Blanchard, R. E. Young, G. Schubert, U. von Zahn, G. Lehmacher, F. S. Milos, and J. Wang, Structure of the atmosphere of Jupiter: Galileo probe measurements, Science, 272, 844-845, 1996.

Seiff A. D., D. B. Kirk, T. C. D. Knight, R. E. Young, J. D. Mihalov, L. A. Young, F. S. Milos, G. Schubert, R. C. Blanchard, and D. Atkinson, Thermal structure Of Jupiter's atmosphere near the edge of a 5-micron hot spot in the north equatorial belt, JGR (this issue) 1998.

Showman, A. P. and A. P. Ingersoll, Interpretation of Galileo probe data and implications for Jupiter's dry downdrafts, Icarus (in press) 1998.

Spilker, T. R., Laboratory measurements of microwave absorptivity and refractivity spectra of gas mixtures applicable to giant planet atmospheres, Ph. D. dissertation, Stanford University, Stanford, California, 1990.

Sromovsky, L., F. A. Best, A. D. Collard, P. M. Fry, H. E. Revercomb, R. S. Freedman, G. S. Orton, J. L. Hayden, M. G. Tomasko, and M. T. Lemmon, Solar and thermal radiation in Jupiter's atmosphere: initial results of the Galileo probe net flux radiometer, Science, 272, 851-854, 1996.

Sromovsky, L., A. D. Collard, P. M. Fry, G. S. Orton, M. T. Lemmon, M. G. Tomasko, and R. S. Freedman., Galileo probe measurements of thermal and solar radiation fluxes in the Jovian atmosphere, JGR (this issue) 1998.

Steffes, P. G. and J. M. Jenkins, Laboratory measurements of the microwave opacity of gaseous ammonia under simulated conditions for the Jovian atmosphere, Icarus 72, 35-47, 1987.

von Zahn, U., and D. M. Hunten, The helium mass fraction in Jupiter's atmosphere, Science 272, 849-851, 1996.

Woo, R., J. W. Armstrong, and W. B. Kendall, Measurements of turbulence in the Venus atmosphere deduced from Pioneer Venus multiprobe radio scintillations, Science, 205, 87-89, 1979.

Table 1. Measurements of probe transmitted power, geometric data, and power received by orbiter. Time is with respect to the probe clock reference designated 'minor frame 0'.

Time (minutes)	LCP power transmit (dBm)	RCP power transmit (dBm)	Probe point (degree)	Space loss (dB)	Orbiter point (degree)	LCP power received (dBm)	RCP power received (dBm)
1.00	43.86	44.12	5.07	-201.95	4.79	-131.06	-132.05
1.50	43.86	44.12	4.93	-201.96	4.64	-131.61	-131.53
2.00	43.86	44.12	4.79	-201.96	4.51	-131.46	-131.97
2.50	43.82	44.12	4.65	-201.96	4.36	-130.99	-131.26
3.00	43.82	44.08	4.50	-201.96	4.22	-131.60	-131.36
3.50	43.82	44.03	4.37	-201.96	4.08	-130.77	-131.27
4.00	43.82	44.03	4.23	-201.96	3.94	-130.95	-131.13
4.50	43.82	44.03	4.09	-201.97	3.80	-131.53	-131.35
5.00	43.73	43.98	3.96	-201.97	3.67	-131.55	-131.74
5.50	43.73	43.98	3.83	-201.97	3.53	-130.72	-130.24
6.00	43.73	43.94	3.70	-201.97	3.39	-130.91	-131.73
6.50	43.73	43.94	3.57	-201.97	3.25	-131.26	-131.96
7.00	43.69	43.89	3.45	-201.98	3.11	-131.17	-131.53
7.50	43.69	43.89	3.33	-201.98	2.97	-130.39	-129.94
8.00	43.64	43.84	3.21	-201.98	2.83	-130.44	-130.46
8.50	43.64	43.84	3.10	-201.98	2.69	-130.19	-130.62
9.00	43.64	43.80	2.99	-201.99	2.55	-130.12	-130.42
9.50	43.64	43.80	2.88	-201.99	2.41	-129.97	-130.78
10.00	43.66	43.75	2.79	-201.99	2.27	-131.22	-131.03
10.50	43.69	43.75	2.69	-201.99	2.13	-130.57	-130.44
11.00	43.69	43.73	2.61	-202.00	1.99	-129.93	-130.25
11.50	43.73	43.70	2.53	-202.00	1.86	-130.02	-130.45
12.00	43.73	43.70	2.46	-202.00	1.72	-130.00	-130.52
12.50	43.69	43.70	2.40	-202.00	1.58	-129.98	-130.59
13.00	43.71	43.65	2.35	-202.01	1.44	-129.96	-130.66
13.50	43.69	43.65	2.31	-202.01	1.30	-129.94	-130.73
14.00	43.69	43.60	2.29	-202.01	1.16	-129.92	-130.80
14.50	43.73	43.60	2.27	-202.02	1.03	-129.91	-130.87
15.00	43.73	43.62	2.26	-202.02	0.89	-129.89	-130.94
15.50	43.69	43.60	2.27	-202.02	0.75	-130.40	-130.77
16.00	43.69	43.62	2.29	-202.03	0.61	-129.84	-130.23
16.50	43.69	43.65	2.32	-202.03	0.48	-129.79	-130.21
17.00	43.69	43.65	2.36	-202.04	0.34	-130.36	-130.20
17.50	43.69	43.65	2.41	-202.04	0.20	-130.10	-130.46
18.00	43.71	43.65	2.47	-202.04	0.06	-129.94	-130.41
18.50	43.73	43.65	2.54	-202.05	0.07	-129.71	-130.64
19.00	43.73	43.68	2.62	-202.05	0.21	-130.17	-130.54
19.50	43.73	43.70	2.71	-202.05	0.35	-130.92	-130.94
20.00	43.69	43.70	2.80	-202.06	0.48	-130.62	-131.21
20.50	43.69	43.75	2.90	-202.06	0.62	-130.07	-130.12
21.00	43.71	43.75	3.01	-202.07	0.76	-130.61	-130.87
21.50	43.69	43.75	3.12	-202.07	0.89	-130.75	-130.79
22.00	43.73	43.80	3.24	-202.08	1.03	-130.28	-130.72
22.50	43.73	43.80	3.36	-202.08	1.17	-130.56	-130.71
23.00	43.73	43.82	3.48	-202.08	1.30	-130.93	-130.54
23.50	43.78	43.84	3.61	-202.09	1.44	-130.45	-130.79
24.00	43.82	43.87	3.74	-202.09	1.57	-130.64	-130.91
24.50	43.82	43.89	3.87	-202.10	1.71	-130.31	-130.62
25.00	43.82	43.89	4.01	-202.10	1.85	-129.90	-130.45
25.50	43.82	43.89	4.14	-202.11	1.98	-130.70	-130.83
26.00	43.86	43.94	4.28	-202.11	2.12	-131.23	-131.27
26.50	43.86	43.94	4.43	-202.12	2.25	-131.29	-131.46
27.00	43.86	43.94	4.57	-202.12	2.39	-131.05	-131.50
27.50	43.86	43.98	4.71	-202.13	2.52	-131.49	-131.40
28.00	43.86	43.98	4.86	-202.13	2.66	-130.84	-131.38
28.50	43.91	43.98	5.01	-202.14	2.79	-131.10	-131.60
29.00	43.91	44.03	5.16	-202.14	2.74	-131.02	-131.41
29.50	43.91	44.03	5.31	-202.15	0.60	-130.90	-131.73
30.00	43.91	44.03	5.46	-202.15	0.46	-132.20	-131.85
30.50	43.91	44.03	5.61	-202.16	0.33	-132.00	-131.83
31.00	43.91	44.03	5.77	-202.17	0.20	-131.77	-131.35
31.50	43.95	44.03	5.92	-202.17	0.06	-131.13	-131.09
32.00	43.97	44.03	6.08	-202.18	0.07	-131.22	-130.90
32.50	43.99	44.03	6.23	-202.18	0.21	-131.66	-131.65
33.00	43.99	44.05	6.39	-202.19	0.34	-131.51	-131.30
33.50	43.99	44.08	6.55	-202.19	0.47	-132.41	-132.19
34.00	44.01	44.08	6.70	-202.20	0.61	-132.13	-131.88
34.50	43.99	44.08	6.86	-202.21	0.74	-132.07	-132.03
35.00	43.99	44.08	7.02	-202.21	0.87	-132.38	-131.96
35.50	43.99	44.08	7.18	-202.22	1.00	-133.15	-132.41
36.00	43.99	44.08	7.34	-202.23	1.14	-132.51	-132.42
36.50	43.99	44.08	7.50	-202.23	1.27	-132.27	-132.02
37.00	43.97	44.08	7.66	-202.24	1.40	-132.65	-132.17
37.50	43.95	44.03	7.82	-202.24	1.53	-132.43	-132.63
38.00	43.95	44.03	7.99	-202.25	1.67	-133.00	-132.51
38.50	43.95	44.03	8.15	-202.26	1.80	-132.57	-132.67
39.00	44.03	44.03	8.31	-202.26	1.82	-133.65	-132.81
39.50	44.03	43.98	8.47	-202.27	0.59	-133.82	-133.09
40.00	44.03	43.98	8.64	-202.28	0.45	-133.07	-132.99
40.50	44.03	43.98	8.80	-202.28	0.32	-134.28	-133.13
41.00	44.01	43.94	8.97	-202.29	0.19	-132.89	-133.48
41.50	44.03	43.89	9.13	-202.30	0.06	-133.94	-133.28
42.00	44.05	43.89	9.30	-202.31	0.07	-133.45	-132.77
42.50	44.07	43.84	9.46	-202.31	0.20	-133.98	-133.61

Table 1. continued

Time (minutes)	LCP power transmit (dBm)	RCP power transmit (dBm)	Probe point (degree)	Space loss (dB)	Orbiter point (degree)	LCP power received (dBm)	RCP power received (dBm)
43.00	44.07	43.84	9.63	-202.32	0.33	-133.91	-133.19
43.50	43.64	43.84	9.79	-202.33	0.46	-135.25	-134.08
44.00	43.50	43.80	9.96	-202.33	0.59	-135.87	-134.67
44.50	43.50	43.80	10.13	-202.34	0.72	-135.63	-135.61
45.00	43.44	43.80	10.29	-202.35	0.85	-135.36	-134.26
45.50	43.34	43.75	10.46	-202.36	0.98	-135.06	-133.70
46.00	43.24	43.75	10.63	-202.36	1.11	-134.95	-136.46
46.50	43.24	43.70	10.79	-202.37	1.24	-136.70	-135.16
47.00	43.07	43.60	10.96	-202.38	1.37	-137.17	-136.54
47.50	42.95	42.56	11.13	-202.39	1.50	-136.91	-136.81
48.00	42.62	37.70	11.30	-202.40	1.63	-137.13	-142.05
48.50	42.39	32.52	11.47	-202.40	1.76	-136.74	-198.64
49.00	42.26		11.64	-202.41	1.78	-137.99	
49.50	42.05		11.80	-202.42	0.57	-139.87	
50.00	41.83		11.97	-202.43	0.44	-139.34	
50.50	41.68		12.14	-202.44	0.31	-139.39	
51.00	41.33		12.31	-202.44	0.19	-138.39	
51.50	41.21		12.48	-202.45	0.06	-139.27	
52.00	40.97		12.65	-202.46	0.07	-138.42	
52.50	40.63		12.82	-202.47	0.20	-139.26	
53.00	40.46		13.00	-202.48	0.32	-140.02	
53.50	40.09		13.17	-202.49	0.45	-140.46	
54.00	39.82		13.34	-202.49	0.58	-139.90	
54.50	39.23		13.51	-202.50	0.71	-140.54	
55.00	38.93		13.68	-202.51	0.83	-140.80	
55.50	38.62		13.85	-202.52	0.96	-141.83	
56.00	38.62		14.02	-202.53	1.09	-142.02	
56.50	39.81		14.20	-202.54	1.21	-141.22	
57.00	42.51		14.37	-202.55	1.34	-138.43	
57.50	41.90		14.54	-202.55	1.47	-139.19	
58.00	39.78		14.71	-202.56	1.60	-141.12	
58.50	35.76		14.89	-202.57	1.75	-143.59	